Journal of Sound and Vibration 391 (2017) 20–34

Contents lists available at ScienceDirect

Journal of Sound and Vibration

journal homepage: www.elsevier.com/locate/jsvi

Modeling and experimental study of a honeycomb beam filled with damping particles

Nazeer Ahmad [a], R. Ranganath [a], Ashitava Ghosal [b,*]

[a] ISRO Satellite Centre, Indian Space Research Organization, Vimanapura Post, Bangalore 560017, India
[b] Department of Mechanical Engineering, Indian Institute of Science, Bangalore 560012, India

ARTICLE INFO

Article history:
Received 5 July 2016
Received in revised form
5 October 2016
Accepted 1 November 2016
Handling Editor: Prof. L. G. Tham
Available online 28 November 2016

Keywords:
Particle damping
Discrete-element method
Honeycomb sandwiched beam
Passive vibration control
Spacecraft structures

ABSTRACT

Honeycomb sandwich laminates which are the basic structural element of spacecraft have inherently low damping. In this paper, we propose to improve the damping characteristics of such structures by adding damping particles in the cells of the honeycomb. This paper presents modeling of a cantilever beam constructed with honeycomb structure with the hexagonal honeycomb cells, filled with particles. The beam is subjected to external dynamic loads and the interactions of damping particles with the walls of the cells and its overall effect on the frequency response function (FRF) and the damping of the beam are obtained. The discrete-element-method (DEM) is used to model the dynamics of the particles in conjunction with the governing equations of motion of the beam and the cell-walls. The particle-particle and particle-wall impact is modeled using Hertz's non-linear dissipative contact model for normal component and Coulomb's laws of friction for tangential component. Contiguous block of cells near the tip of the cantilever beam were filled with the damping particles and the beam was excited with a random signal near the fixed end. The damping and transfer functions obtained experimentally are compared to those obtained from the mathematical model and they are found to match very well. Further the model was used to study the effect of fill fraction, mass ratio, and the level of excitation signal on transfer function. Depending on the mass ratio and fill fraction, significant reductions in vibration levels are observed.

1. Introduction

Sandwich honeycomb laminates are extensively used for designing the bus and other components of a spacecraft. These structures are light and have inherently low damping. The damping performance could be improved by inserting granules called damping particles in the empty cells of the honeycomb core [1–4]. This method of introducing damping is called particle impact damping (PID). The PID is a form of passive vibration control technique wherein the energy of a vibrating system is dissipated through impact and friction in the form of heat, elastic wave, sound etc. The impact damping technologies usually involve either attaching a container filled with damping particles (spherical balls of aluminium, steel, tungsten, carbide etc.) to vibrating structure or filling a cavity in the host structure drilled at appropriate location [5,6]. Traditionally, in a PID technique, a single spherical mass (impactor) is constrained to move between two stoppers or in an enclosure. The PID technique has been studied extensively, both theoretically and experimentally, for its effect on structural

* Corresponding author.
E-mail address: asitava@mecheng.iisc.ernet.in (A. Ghosal).

http://dx.doi.org/10.1016/j.jsv.2016.11.011
0022-460X/

response with respect to parameters such as mass ratio, clearance, material and dimension of the particle, nature of excitation and level, and for its stability, and its nonlinear behavior by several researchers [7–10]. The impact force in the PID is large and introduces shock and noise in the system along with surface degradation. The use of the multiple particles or soft particles could reduce the impact loads and its undesirable effects on host structure. This modification of the classical PID is also referred to as particle damping (PD). The PD being very simple in construction, insensitive to environment, low cost, and effective over wide temperature and frequency range could replace the conventional viscous and viscoelastic dampers, particularly in harsh environmental conditions. The PD has been successfully used for vibration attenuation in wide range of applications like civil structures against wind and earthquake loads [11], turbine blades, machine tools, space shuttle and aerospace structures [12–15]. The energy dissipation mechanism in PD is highly nonlinear and depends on host of parameters, predominantly: size, shape and number of particles and material of the particles, enclosure relative geometry and material, mass ratio, location of PD with respect to structural mode and the level of excitation.

The energy dissipation and its effect on structural response in particle damping depend on the relative proportion of different parameters. It is extremely difficult to evolve a model to capture all the interactions taking place. The main modeling techniques available in literature are: (a) multiphase flow method (see Wu et al. [16]) where the theory of gases is used to build a model to evaluate the particle damping by formulating expressions for drag forces equivalent to viscous damping and Coulomb friction damping, (b) single degree of freedom (SDOF) spring-mass-dashpot system model (see, for example, Liu et al. [17], Michon et al. [4]) which analyzes the particle damping problem by attaching a SDOF oscillator with equivalent stiffness, viscous damping and mass to the primary structure and (c) the discrete element method (DEM) which track the motion and contact history of each particle in the assembly and estimates the damping due to collision between the particles and with the walls. The DEM after the seminal work of Cundall and Strack [18] is now an established tool for analyzing the dynamic behavior of assemblies of particles under different loads and boundary contacts. DEM is based on Newtonian mechanics where equation of motion of each particle is established by considering the contact forces and moments from the surrounding particle and boundary contacts or any other source. The accuracy of DEM depends on accuracy of contact model and the time step. The time step is very crucial since at each time step new contacts may be established and old contacts may be broken and therefore new set of equations are generated. The basic underlying assumption in selection of time step is that the disturbance should not propagate farther from its immediate neighbor. Although it is computationally very expensive, many researchers have used DEM to analyze the particle damping problem. Saeki [19,20], studied the particle damping for single degree-of-freedom primary system under sinusoidal excitation and reported good agreement between DEM and experiment. The authors reported that the mass ratio, cavity size and particle size influence the damping of the system. Wong et al. [21], Mao et al. [22] used DEM to predict the energy dissipation in particle damping (PD) that compared well with the experiment. Fang et al. [23] proposed an improved DEM for PD analysis which was significantly faster because of limiting the contact search space and optimal time step. Lu et al. [24] carried out the parametric studies on the performance of horizontal and vertical single-degree-of-freedom (SDOF) and multi-degree-of-freedom (MDOF) primary system under random loads using DEM.

Very limited studies on the damping and response behavior of sandwich beam with honeycomb core filled with damping particle are available in literature [1,4,25–27]. Wang and Yang [1] carried out experimental study of a laminated honeycomb beams filled with solder balls as damping particles. They reported reduction of response without damaging the cells and bonding. Michon et al. [4] studied the effect on the damping characteristic of a cantilever beam filled with viscoelastic balls. They experimentally obtained the parameters of an equivalent dynamics oscillator. The viscous equivalent damping was shown to be a function of filling ratio and excitation frequency based on the measurement of the force and displacement of the shaker exciting a small coupon. Significant improvement in the damping of second mode of a cantilever beam was reported.

There is no literature available modeling particle-cell level interaction and the dependence of the response of structure on the parameters of the damping particles filled in the cells of the core. In this paper we present the modeling of the coupled dynamics of the particle in the honeycomb cell by DEM. The motion of the cell walls is obtained from the motion of the center of the cell that is assumed to be lying on the neutral axis of the beam. The particle-wall interaction are modeled using Hertz nonlinear dissipative contact model in conjunction with the Coulomb's law of friction. A cantilever beam was

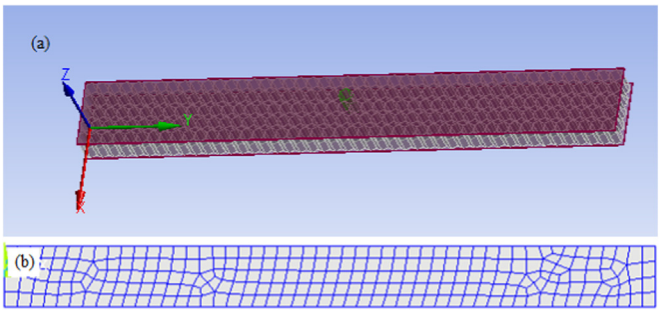

Fig. 1. (a) Sandwich honeycomb beam (b) Finite element model of the beam.

considered for numerical and experimental study. The transfer function obtained experimentally and analytically is compared and after validating the model, it is used to study the damping behavior with respect to filling fraction mass ratio, and input excitation level.

This paper is organized as follows: In Section 2, we present the mathematical formulation where the relevant equations and the model used for numerical simulations are presented. In Section 3, we present experimental results and show that the experimental results validate the model. The effect of various parameters, such as fill fraction, and their effect on the resultant damping are obtained by numerical simulations of the validated model. Finally Section 4, presents the conclusions of this work.

2. Mathematical formulations

Fig. 1(a) shows a laminated beam consisting of two aluminum face sheets sandwiching an aluminum honeycomb core. The hexagonal cells of the honeycomb are filled with the damping particles at strategically chosen locations. The finite element equations of motion of the beam treated with damping particles can be written as

$$\mathbf{M}\ddot{\mathbf{w}} + \mathbf{C}\dot{\mathbf{w}} + \mathbf{K}\mathbf{w} = \mathbf{f}^d + \mathbf{f}^e \tag{1}$$

where $\mathbf{M}$, $\mathbf{K}$ and $\mathbf{C}$ are the mass, stiffness and damping matrices, respectively, $\mathbf{f}^d$ represents the force vector resulting from the impact of damping particles and represents the link between the dynamics of the beam and the dynamics of the particles, $\mathbf{f}^e$ is the external force vector other than particle damping force and $\mathbf{w}$ is the displacement of the neutral axis of the beam in the direction of $\mathbf{z}$. A dot over a variable represents the time derivative.

A modal analysis of the beam is carried using the ANSYS software. The beam is modeled by a 4 node composite shell element, shell 181. The meshed beam is shown in Fig. 1(b). The honeycomb core is modeled as an orthotropic material whose properties are obtained experimentally. The finite element equations of motion, Eq. (1), can be recast into modal space using the modal vectors and normal mode frequency obtained from ANSYS, assuming the inherent damping to be of Rayleigh mass and stiffness-proportional type and invoking the mass and stiffness orthogonality relations. We get

$$\ddot{\mathbf{q}}_i + 2\xi_i\omega_i\dot{\mathbf{q}}_i + \omega_i^2\mathbf{q}_i = \frac{1}{m_i}\sum_{j=1}^{N}(\boldsymbol{\psi}_i^T(y_j)\mathbf{f}_j^d + \boldsymbol{\psi}_i^T(y_e)\mathbf{f}^e) \tag{2}$$

where $\mathbf{q}_i$ is the modal coordinate, $\boldsymbol{\psi}_i$ is the mass normalized modal vector and m_i is generalized mass;ξ_i and ω_i are the modal damping ratio and normal mode frequency.

2.1. Computing the impact damping forces

The damping particles inside the cells exchange momentum with the cell walls and with each other through collisions and friction as the beam vibrates, shown in Fig. 2(a). Let n be the number of particles in cell j at location $y = y_j$ and $-f_{iw}^d$ be the force acting on the wall of the cell due to impact of particle i. Then the equivalent force f_j^d is assumed to be acting at the center of the cell due to impact and friction of all the particles in the cell j can be represented as:

$$\mathbf{f}_j^d = -\sum_{i=1}^{n}\mathbf{f}_{iw}^d(y_j, t) \tag{3}$$

The equivalent moment at center of the cell due to impact forces is ignored as the dimensions of the cells are very small. The force $\mathbf{f}_j^d$ is expected to be predominantly in the direction z as the significant contribution in Eq. (3) is due to the impact of the particle with bottom and top walls of the cell or with the sidewalls with large impact angle. Therefore, the equivalent

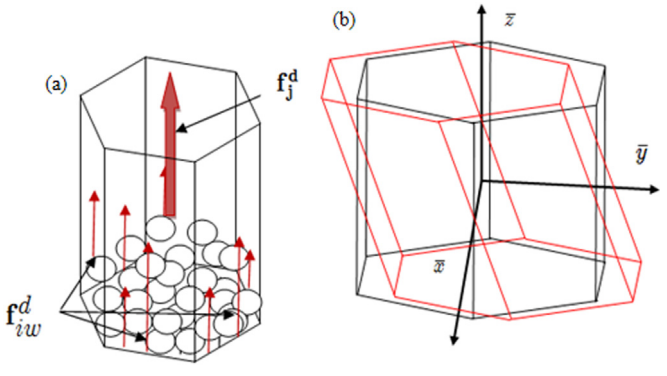

Fig. 2. (a) An isolated cell with damping particle and impact forces. (b)An isolated deformed cell with a local coordinate system at the centre of the cell.

force from each cell is assumed to be a transverse point force acting on the beam.

The impact force on the beam due to collision of particle with the cell walls depends on the relative position and velocity of the damping particles with respect to cell walls along with the material properties. Therefore the motion history of each particle and the position and velocity of the points of impact is required to be known.

The equation of motion of the particle i that is in contact with n_1 number of surrounding particles and n_2 points with cell walls can be written as:

$$m_{pi}\ddot{\mathbf{p}}_i = -m_{pi}g + \sum_{j=1}^{n_1}\mathbf{f}_{ij} + \sum_{w=1}^{n_2}\mathbf{f}_{iw} \tag{4}$$

$$\mathbf{I}_i\ddot{\mathbf{\Phi}}_i = \sum_{j=1}^{n_1}\left(r_i - \frac{\delta_{ij}}{2}\right)\mathbf{n}_{ij}\times\mathbf{f}_{ij} + \sum_{j=1}^{n_2}(r_i - \delta_{iw})\mathbf{n}_{iw}\times\mathbf{f}_{iw} \tag{5}$$

where m_{pi}, r_i, and $\mathbf{I}_i$ are the mass, radius and mass moment of inertia of the particle i, respectively; $\mathbf{p}_i$ is the position vector of the center of mass and $\mathbf{\Phi}_i$ the angular displacement of the particle i. The unit vectors $\mathbf{n}_{ij}$ and $\mathbf{n}_{iw}$ point from the center of the particle i towards the center of the particle j and towards the point of contact with cell wall. The acceleration due to gravity is represented by $\mathbf{g}$ and $\mathbf{f}_{ij}$ and $\mathbf{f}_{iw}$ are the forces on particle i due to interaction of particle j and by the wall of the cell, respectively. The indentations between particles i and j and particle i and the wall of the cell when they are in contact with each other are represented by, δ_{ij} and δ_{iw}, respectively, and are given as

$$\delta_{ij}^n = r_i + r_j - \left|\mathbf{p}_i - \mathbf{p}_j\right| \tag{6}$$

$$\delta_{iw}^n = r_i - \left|\mathbf{p}_i - \mathbf{p}_w\right| \tag{7}$$

where the position vector of the contact point on the wall of the cell $\mathbf{p}_w$ and the unit vector $\mathbf{n}_{iw}$ is obtained from the information of the displacement and rotation of the geometric center of the cell that lies on the neutral axis of the beam.

It is assumed that the cell walls remain plane but undergoes rotation as the beam deforms. The deformation in the wall due to impact is not taken into account. Let the cell j of the honeycomb is at location $y = y_j$ and the deflection and slope of the neutral axis of the beam at that point are w_j and $\partial w/\partial y|_{y=y_j}$, respectively. Then the equation of planes defining the deformed walls of the cell as shown in Fig. 2(b) can be written with respect to a frame of reference attached to the geometric center of the cell as:

$$\bar{z} \pm \frac{h}{2} = 0 \tag{8}$$

$$\bar{y} \pm \sqrt{3}\left(\bar{x} + R\right) + \frac{\partial w}{\partial y}\bar{z} = 0 \tag{9}$$

$$\bar{y} \pm \sqrt{3}\left(\bar{x} + R\right) - \frac{\partial w}{\partial y}\bar{z} = 0 \tag{10}$$

$$\bar{y} + \frac{\partial w}{\partial y}\bar{z} \pm \frac{\sqrt{3}}{2}R = 0 \tag{11}$$

where R is the radius of circumscribing cylinder of regular hexagon representing the honeycomb cell and the coordinates are related to the global by relations:$\bar{x} = x$, $\bar{y} = y - y_j$ and $\bar{z} = z - w_j$.If the Eqs. (8–11) were represented by: $ax + by + cz + d = 0$ then δ_{iw} is given as

$$\delta_{iw} = \frac{ax_i + by_i + cz_i + d}{\sqrt{a^2 + b^2 + c^2}} \tag{12}$$

where the $\begin{bmatrix} x_i & y_i & z_i \end{bmatrix}$ is the coordinate of the center of the particle i. The coordinates of the point of contact can be obtained from

$$(x_w - x_i)\mathbf{i} + (y_w - y_i)\mathbf{j} + (z_w - z_i)\mathbf{k} = |\delta_{iw}|\mathbf{n_{iw}} \tag{13}$$

where $\begin{bmatrix} x_w & y_w & z_w \end{bmatrix}$ is the coordinate of the point of contact and $\mathbf{n}_{iw}$ is the unit vector pointing from centre of particle i to the contact point on the plane. The unit vector $\mathbf{n}_{iw}$ is given as

$$\mathbf{n}_{iw} = \frac{a\boldsymbol{i} + b\boldsymbol{j} + c\boldsymbol{k}}{\sqrt{a^2 + b^2 + c^2}} \tag{14}$$

The Eq. (12) can be solved from the knowledge of variables $w_j = \sum_{i=1}^{n}\psi_i(y_j)q_i(y_t)$ and $\left.\frac{\partial w}{\partial y}\right|_{y=y_j} = \sum_{i=1}^{n}q_i\frac{\partial \psi_i}{\partial y}$ that is required to

be known for contact detection and contact force computation.

The contact force between particles and particle-wall consists of tangential and normal components given as

$$\mathbf{f}_{ij} = \mathbf{f}_{ij}^{n} + \mathbf{f}_{ij}^{t} \tag{15}$$

The normal component of contact force $\mathbf{f}_{ij}^{n}$ is modeled as the sum of elastic and dissipative forces as the impact event always results in elastic or elastic-plastic deformation and dissipation of some kinetic energy. The low velocity impacts that take place between the particles and the particle-walls allow considering the only the elastic - dissipative models. The force-indention ($\mathbf{f}_{ij}^{n} - \delta_{ij}^{n}$) relation depends on the geometry and material of impactor and target, magnitude of indentation and the relative velocity. The widely used model for normal contact force is the Kelvin-Voigt [28] that combines a linear spring with linear damper in parallel as($f_{ij}^{n} = k\delta_{ij}^{n} + D\dot{\delta}_{ij}^{n}$). Although there are many drawback in this model, such as the contact force is not continuous in the beginning of the contact process due to the damping term being proportional to $\dot{\delta}_{ij}^{n}$ which is not possible in real physical process, the normal force must be zero when $\delta_{ij}^{n} = 0$. The Kelvin-Voigt model gives uniform dissipation of energy in approach and a restitution phase which is against the established nonlinear asymmetrical behavior whereby most of the dissipation happens during the approach, particularly in low coefficient of restitution impacts. Moreover, at the end of restitution phase relative velocity becomes negative which implies that the impacting bodies are attracted towards each other, again non-realistic phenomenon. However, many researchers have used Kelvin-Voigt model, or a slightly modified model in which the linear elastic force component was replace by a more accurate term based on Hertz contact theory and linear damping component, in particle damping problems, that retains all the weaknesses of the Kelvin-Voigt model. In this work, a nonlinear contact force and damping model proposed by Tsuji et al. [29] is used. This model has been used by several researchers [19,20,23] in a particle damping problems predicting reasonably good results. The $\mathbf{f}_{ij}^{n}$ is given as

$$\mathbf{f}_{ij}^{n} = -(k_n(\delta_{ij}^{n})^{3/2} + \alpha\sqrt{m_{ij}^{*}k_n}(\delta_{ij}^{n})^{1/4}\dot{\delta}_{ij})\mathbf{n}_{ij} \tag{16}$$

where $\dot{\delta}_{ij}^{n}$ is the normal relative velocity of the center of particle i with respect to the center of particle j and α is the damping constant and a nonlinear function of the normal coefficient of restitution e_n [29], given as

$$\alpha = -\ln(e_n)\sqrt{\frac{5}{\ln(e_n)^2 + \pi^2}} \tag{17}$$

The elastic Hertz's constant k_n for spherical impacting bodies and sphere-plan wall is given by Eqs. (18) and (19), respectively as

$$k_n = \frac{4}{3}\sqrt{\frac{r_i r_j}{r_i + r_j}}\frac{E_i E_j}{(1-\upsilon_j^2)E_i + (1-\upsilon_i^2)E_j} \tag{18}$$

$$k_n = \frac{4}{3}\sqrt{r_i}\frac{E_i E_w}{(1-\upsilon_w^2)E_i + (1-\upsilon_i^2)E_w} \tag{19}$$

where E_i,ν_i and E_w ν_w are the Young's modulus and Poisson's ratio of the particle i and the wall of the cell respectively. The equivalent mass m_{ij}^{*} in Eq. (16) is defined as

$$m_{ij}^{*} = \frac{m_i m_j}{m_i + m_j} \tag{20}$$

Modeling the tangential component $\mathbf{f}_{ij}^{t}$ of the contact force of compliant impacting bodies is still evolving and a current research area. Mindlin-Deresiewicz [30] developed an incremental procedure and a series of assumption regarding the history of loading and unloading to relate the tangential force to tangential displacement through an incremental tangential stiffness. This model takes into account the tangential compliance and correctly describes the sticking and gross-sliding phases in the contact process. A more rigorous and accurate model was developed by Maw et al. [31] which relaxed many assumptions of the Mindlin-Deresiewicz model as it does not make any assumption regarding the loading history. This model discretizes the contact area into concentric annuli and normal and tangential forces and displacements are evaluated at each time step, for sticking annuli, the elastic theory and for sliding annuli the Coulomb's friction theory was used, respectively. Maw's theory accurately predicts the mechanics of contact phenomenon and the post contact the dynamic behavior of impacting bodies. It clearly identifies the phases of micro-slip and gross sliding. Other models for tangential force, which are modification of these two models, can be found in [32–34].

The simplest approach is to model using the Coulomb's law of sliding friction [35]. This is easiest to implement and most efficient among all the models for tangential force component computation in a contact process. However, it gives grossly erroneous results of post impact dynamics when the angle of incidence is small (less than a critical value that depends on material properties of impacting bodies – for ordinary material it is around 30 degree, see [35]). Moreover, the tangential force oscillates due to change in the direction of the tangential velocity. It captures only gross-sliding and rolling phases and fails to predict the negative bounce for certain angles of incidence.

The choice of a particular model for DEM application is usually based on two considerations: (1) the computational time

considering the large number of particles and (2) the accuracy of the model. The model of Maw et al. [31] is mathematically rigorous and accurate but computationally very expensive making it impractical to use in DEM applications whereas Coulomb's model is fast but only moderately accurate. The Coulomb's law has been used by many researchers in DEM for predicting vibration responses [11,19,20,23,24,36] and is used in this work. The Coulomb friction force is given as

$$\mathbf{f}_{ij}^{t} = -\mu\left|\mathbf{f}_{ij}^{n}\right|\frac{\mathbf{V}_{ij}^{t}}{\left|\mathbf{V}_{ij}^{t}\right|} \tag{21}$$

where μ is the coefficient of friction and $\mathbf{V}_{ij}^{t}$ is the relative tangential velocity of contact point. Let $\mathbf{v}_i$ and $\mathbf{v}_j$ be the linear velocity of the CM sand $\boldsymbol{\omega}_i$ and $\boldsymbol{\omega}_j$ be the angular velocity of particles i and j, respectively. Then the relative velocity at the centre of contact area of particle i with respect to particle j can be written as

$$\mathbf{V}_{ij} = \mathbf{v}_i - \mathbf{v}_j + (r_i\boldsymbol{\omega}_i + r_j\boldsymbol{\omega}_j) \times \mathbf{n}_{ij} \tag{22}$$

The tangential component $\mathbf{V}_{ij}^{t}$ and can be written as

$$\mathbf{V}_{ij}^{t} = \mathbf{V}_{ij} - (\mathbf{V}_{ij}.\ \mathbf{n}_{ij})\mathbf{n}_{ij} \tag{23}$$

The equations of motion of the beam and particles, Eq. (2), Eqs. (4) and (5), respectively, are solved simultaneously. The 4th order Runge-Kutta method (RK-4) was used for integration in the MATLAB software. The DEM formulation assumes that the motion of any particle is affected by its immediate neighborhood contacts only. This implies that the time step chosen to integrate the equations of motion should be small enough so that the disturbance does not propagate beyond its immediate neighbor in single step and it must at least an order less than the contact period. In this work a time step of 10^{-6}s is used. As the DEM computation progresses, the new contacts are formed and old contacts are broken. Therefore, at each time step contact detection is performed and this consumes most of the time. When contact detection of particle with cell wall is performed, the cell walls are assumed to be plane and the local vibration of the cell is ignored since the stiffness of local indentation is much higher than the bending stiffness of the cell wall. Lu et al. [24] reported that a frequency ratio of greater than 20 is appropriate to represent a stiff barrier whereby the compliance of the barrier can be ignored.

3. Experimental investigation and model validation

3.1. Experimental setup

A honeycomb sandwich beam of dimensions, length L = 850 mm, width W = 80 mm and thickness t = 26.4 mm was used for experimental study. The thickness of the top and bottom face sheets of the beam is 0.5 mm and the honeycomb core is 25.4 mm. The face sheets and core are made of aluminum. The material properties of the core and face sheets are given in Table 1. The elastic properties of the honeycomb core were obtained experimentally from the coupon level tests.

Figs. 3 and 4 show the experimental setup and test schematic, respectively. The cantilever beam was excited by a modal shaker (make: M B Dynamics, model: 2050 A, Force rating: 100 N) fixed at a distance y = 275 mm from the fixed end. This location was chosen to excite multiple bending modes. The location is not at the nodes of any bending mode in the frequency range of interest (less than 1000 Hz).

A high sensitivity impedance head (make: PCB, model: 288D01) for measuring the input acceleration and force was attached at the top of stinger connecting the modal shaker to the beam. The acceleration response at five locations along the length of the beam was measured using accelerometers (make: B & K, Model: 4517-002, sensitivity approximately 10 mV/g). The accelerometers are separated by A_y = 100 mm from each other. A 32 channel data acquisition system (DAS) from LMS was used for data acquisition and LMS Test Lab software was used for data processing. An area of 2400 mm^2 is identified near the tip of the beam for filling the damping particles. This location was chosen so that all the bending modes of a cantilever beam have significant motion near the tip. The area chosen covers 80 cells and can accommodate 2800 particles of 1.25 mm radius when filled at 100%. The reason for choosing a small patch rather than entire specimen unlike [1,4] for filling the damping

Table 1
Material and elastic properties of the core and face-sheets.

Properties	Face-sheet (Aluminium (AA 2024 T3)	Honeycomb core
Density, kg/m^3	2800	32
Young's modulus, N/m^2	72×10^9	$E_{xx}=E_{yy}=E_{zz}=10000$
Poisson's ratio	0.33	$v_{xy}=v_{yz}=v_{xz}=0.3$
Shear modulus, N/m^2	–	$G_{xy}=1000$ $G_{yz}=0.89\times10^8$ $G_{xz}=0.89\times10^8$
Diameter of the circumscribing circle of a hexagonal cell, mm	–	6

Fig. 3. Setup for experimental study.

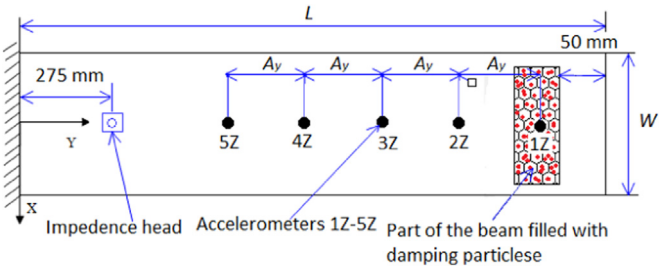

Fig. 4. Schematic of test setup (Plan view, not to scale).

particles is that it might not be effective at all locations and would unnecessarily add mass to the structure.

3.2. Experimental characterization of the beam

The modal characteristic of the beam without the damping particle was obtained by subjecting it to a broadband Gaussian random vibration generated by the modal shaker. The power spectral density (PSD) of the input force signal is flat 0.02 N^2/Hz over a bandwidth of 5 Hz to 5 kHz and the RMS value was 10 N. A 10 s slice of the input force measured by impedance head is given in Fig. 5.

The acceleration response data from the 5 accelerometers mounted on the beam was acquired at 5ks/s that is approximately 5 times the frequency of interest (i.e. 1 kHz) and well above the sampling rate prescribed by Nyquist criterion. The experimental data was acquired for duration of 40 s and processed in blocks of 4 s to get a frequency resolution of 0.25 Hz that is sufficient to study the effect of impact damping on the transfer function and resonance peaks. The H_1 transfer function defined as the ratio of the cross - PSD of input force signal, output acceleration signal to auto- PSD of input force signal, also called accelerance, is used for estimation of the modal properties of the beam such as damping ratio, resonance frequency, and normal mode shapes. The transfer functions from the time domain data of the 5 accelerometers mounted along the length of the beam was estimated with the following parameters: block size, 4 s; window, Hanning; averages, 16

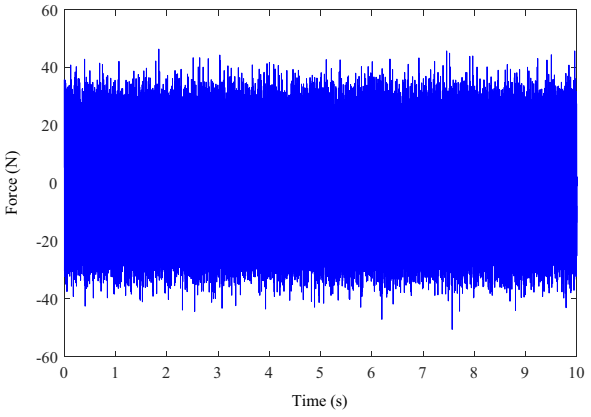

Fig. 5. The random input force.

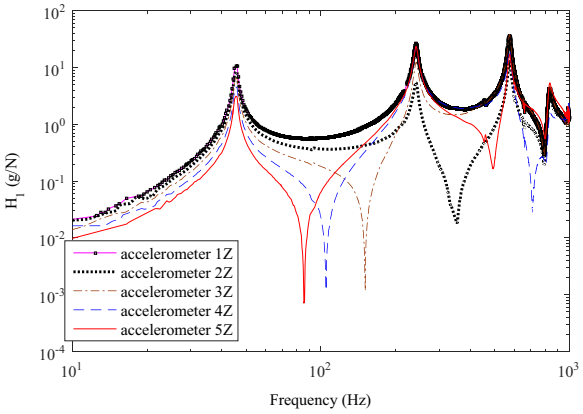

Fig. 6. Transfer functions of the bare beam at locations 1Z-5Z.

and overlapping,50%; are given in Fig. 6. The Welch's method was used for estimating the auto-PSD and cross-PSD for computing the transfer functions given in Fig. 6.

The modal damping of the beam is obtained from the transfer functions given in Fig. 6 by half power bandwidth method [37]. The damping ratio at different locations for the same mode varies marginally. However, the damping ratio for all the modes at location 1Z is considered to be representative of the mode and will be used for comparison and further study. The damping ratio for 4 bending modes excited below 1 kHz is given in Table 2. The normal mode frequency from the FEM is also presented in the Table 2.

3.3. Updating the FEM model of the beam

The dynamic model of beam represented by Eq. (2) is updated using the experimental data available for the natural frequency, mode shapes and damping ratio. The modal data for the 4 bending modes is incorporated in the dynamic model to get better representation of the beam dynamics. The updating procedure is described as follows.

The receptance FRF, H_{re}, defined as the ratio of the Fourier transform of the output displacement at location r to the Fourier transform of the input force excitation at location e for a system described by Eq. (1) can be written as [38]

$$H_{re}(\omega) = \sum_{i=1}^{N} \frac{\psi_{ri}\psi_{ei}}{m_i(\omega_i^2 - \omega^2 + 2j\xi_i\omega_i^2)} \tag{24}$$

where ψ_{ri} and ψ_{ei} are the i the modal vector at response point and excitation point respectively, and m_i is the i^{th} generalized modal mass. The magnitude of the transfer function at ith resonance can be deduced from Eq. (24) as

$$|H_{re}|_i = \frac{\psi_{ri}\psi_{ei}}{2m_i\xi_i\omega_i^2} \tag{25}$$

The ith generalized modal mass m_i can be obtained from Eq. (25) as all the variable can be input from the experimental data. The magnitude of receptance at the ith mode $|H_{re}|_i$ is $1/\omega_i^2$ times the magnitude of accelerance FRF given in Fig. 6. Having obtained the modal vectors at response points and with the availability of the frequency and the damping for the first four modes, the mass and stiffness matrices in Eq. (1) are corrected using the direct model updating methods [39,40]. The modal model is obtained from the updated equations by invoking mass and stiffness orthogonality relations and can be partitioned as follows

Table 2
FEM and experimental modal test results on empty beam.

Frequency (FEM) (Hz)	Frequency (Test) (Hz)	Damping ratio (Test)	Mode shape description
44.8	45.6	0.014	1st Bending mode
240.1	241.7	0.016	2nd Bending mode
576.6	575.0	0.011	3rd Bending mode
860.8	835.5	0.017	4th Bending mode

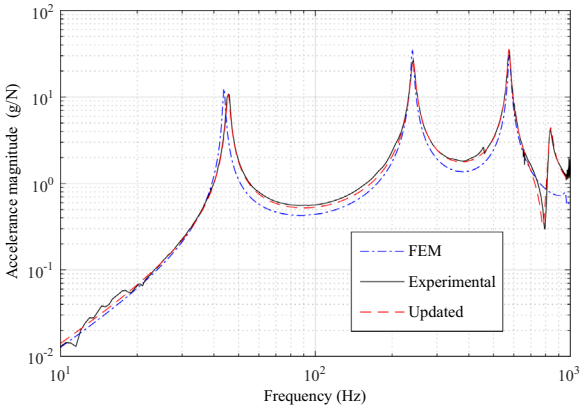

Fig. 7. Transfer function of beam without PD.

$$\begin{bmatrix} \ddot{\mathbf{q}}_i \\ \ddot{\mathbf{q}}_k \end{bmatrix} + \begin{bmatrix} 2\xi_i\omega_i & 0 \\ 0 & 2\xi_k\omega_k \end{bmatrix} \begin{bmatrix} \dot{\mathbf{q}}_i \\ \dot{\mathbf{q}}_k \end{bmatrix} + \begin{bmatrix} \omega_i^2 & 0 \\ 0 & \omega_k^2 \end{bmatrix} \begin{bmatrix} \mathbf{q}_i \\ \mathbf{q}_k \end{bmatrix} = \begin{bmatrix} \frac{1}{m_i} \sum_{j=1}^{N} \mathbf{f_j \psi_i}(y_j) \\ \frac{1}{m_k} \sum_{j=1}^{N} \mathbf{f_j \psi_k}(y_j) \end{bmatrix} \tag{26}$$

where i and k represent the number of experimental and FEM modes. The transfer function at location 1Z obtained from the updated Eq. (26) is presented in Fig. 7 along with the transfer function obtained by FEM and tests. The transfer functions from the updated model are closely matching with the test.

3.4. Experimental results and numerical simulation comparisons

Once the dynamic model of the empty beam is updated with the experimental data, three cases of experimental and simulation study on the beam, filled with acrylic damping particle with different fill fraction at the location shown in the Fig. 4, was conducted and the results are compared. Acrylic balls are chosen as they have low density and therefore would not add significant mass to the system. The material and physical properties of the acrylic particles are given in Table 3.

The beam was made to vibrate for all three cases using the random input of the same PSD profile as used in the characterization tests. The transfer functions from test and simulation, at location 1Z (see Fig. 4), for different fill fractions are given in Fig. 8. The modal frequency and the damping ratios were obtained from these transfer functions. The damping from the FRF data is computed using half power bandwidth method. A comparison of damping ratio between computed and experimentally obtained is given in Table 4. For Mode 3 and 4, rotations of the cross-section should come into play. However, the frequency matches closely due to background damping.

3.5. Effect of the fill fraction

Conventionally, fill fraction is defined as the ratio of the volume of the particles to the volume of the container. However, in context of particle damping literature and in this work, wherever the fill fraction is referred to, it is the ratio of the volume of container randomly filled with particles to the entire volume of the container.

Table 3
Material and physical properties of the damping particles.

Parameters	Value
Radius	1.25 mm
Density	1180 kg/m^3
Young's modulus	2.0×10^9 Pa
Poisson's ratio	0.35
Coefficient of friction (acrylic-acrylic)	0.52
Coefficient of friction (aluminium-acrylic)	0.45
Coefficient of restitution	0.9

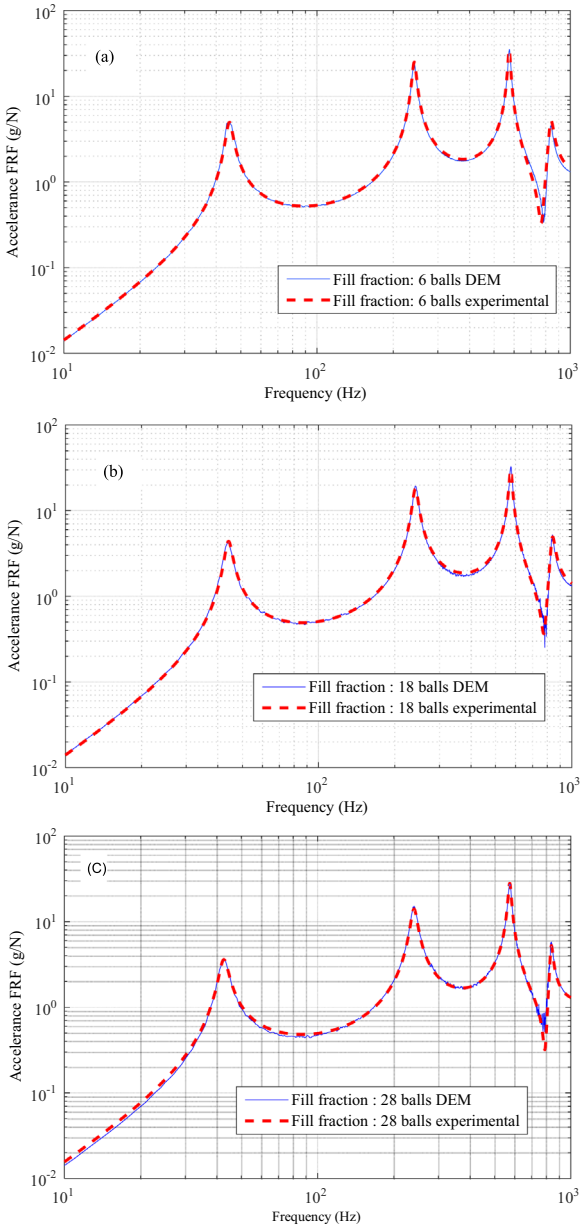

Fig. 8. Comparison of computed and experimental accelerance FRF for different fill fractions (a) 6 balls (20%) (b) 18balls (60%) and (c) 28 balls (93%).

A simulation result for different fill fraction is presented in Fig. 9. As the fill fraction is increased the mass of damping particles and number of particles also increases. Therefore, the transfer function reflects the combined effect of increased mass and number of particles. The effect is different at different frequency. The amplitude at first mode drops by 66.6% from 10.8 g/N to 3.6 g/N, damping ratio increases from 1.4% to 4.3%. For the second mode, at around 240 Hz, the resonance peak decreases from 26.86 g/N to 14.96 g/N and in the third mode from 35.5 g/N to 28.5 g/N. The fourth mode does not undergo any significant change. However, for higher fill fraction a small increase in the peak value is observed in the fourth mode. The likely reason for this phenomenon could be the redistribution of energy from off resonance region to resonance zone. There is very small shift in the frequency owing to increase in the mass. The decrease in the response is monotonic for the first three modes as numbers of particles are increasing which result in more number of collisions taking place.

3.6. *Effect of mass ratio*

The numerical study on the effect of mass ratio, defined as the ratio of the mass of the damping particles to the mass of

Table 4
Comparison of computed and test results.

Mode description	Frequency (Test) (Hz)	Frequency (Computed) (Hz)	Damping ratio (Test)	Damping ratio (Computed)	Error (%)
Filling fraction 20% (6 balls in each cell)					
1st Bending mode	45.00	45.00	0.031	0.030	3.226
2nd Bending mode	240.00	241.50	0.020	0.021	-5.000
3rd Bending mode	574.25	575.00	0.012	0.011	8.333
4th Bending mode	835.00	835.00	0.023	0.021	8.696
Filling fraction 60% (18 balls in each cell)					
1st Bending mode	44.00	43.00	0.044	0.042	-4.545
2nd Bending mode	240.00	240.00	0.027	0.028	3.704
3rd Bending mode	574.00	575.00	0.016	0.014	-12.500
4th Bending mode	834.00	835.00	0.021	0.020	-4.762
Filling fraction 93% (28 balls in each cell)					
1st Bending mode	42.25	41.50	0.043	0.043	0.000
2nd Bending mode	240.00	240.00	0.030	0.029	-3.333
3rd Bending mode	574.00	574.00	0.015	0.014	-6.667
4th Bending mode	830.50	830.00	0.014	0.013	-7.143

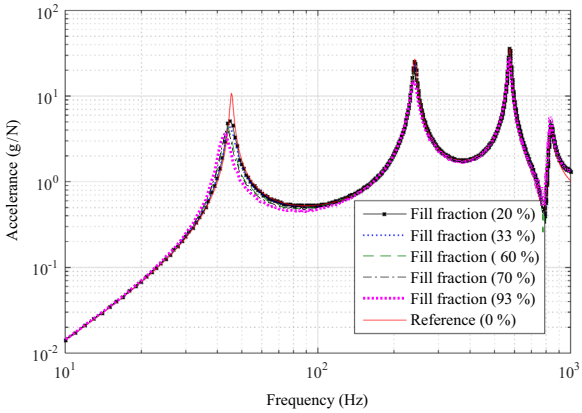

Fig. 9. Effect of fill fraction on TF.

the beam, was conducted by varying the mass ratio from 0.019 to 0.155 (i.e. 8 times the original mass of the particles). Filling each cell of the beam at location shown in the Fig. 4 with 12 balls of acrylic material of 1mm radius gives a mass ratio of 0.019. To study the effect of mass ratio alone the density of the damping particles is varied keeping all other parameters constant. The variation in density allows the fill fraction as well as number of particles to remain constant and therefore the

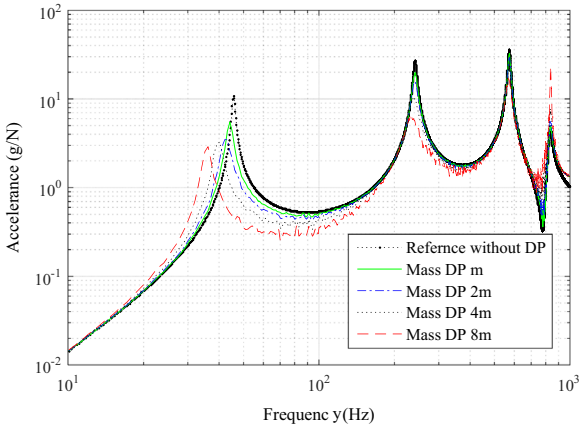

Fig. 10. Effect of mass ratio.

Table 5
Effect of mass ratio.

mass ratio	1st mode	Reduction (%)	2nd mode	Reduction (%)	3rd mode	Reduction (%)
0	10.8	0.0	26.9	0	35.5	0
0.019	5.5	49.1	19.9	26.0	32.7	7.9
0.038	3.5	67.6	15.7	41.6	29.5	16.9
0.076	3.3	69.4	10.5	61.0	23.3	34.4
0.152	2.9	73.1	6.3	78.9	17.2	51.5

changes in the transfer function can be attributed to the change in mass ratio alone. Fig. 10 shows the effect of mass ratio. It can be seen that as the mass ratio increases the resonance peak monotonically decreases at first three modes while its effect on 4th bending mode is negligible except for the last load case.

At the 4th bending mode, the resonance peak increases for mass ratio of 0.152. The likely reason could be the redistribution of energy. The percentage of resonance peak for the 2nd mode is highest at 78.9% and lowest for the 3rd mode at 51.5%. A frequency shift is also observed in all bending modes: first mode shifts from 45.5 Hz to 36.0 Hz whilst the 2nd and 3rd mode shifts from 241.5 Hz to 232.0 Hz and 575.0 Hz to 570 Hz, respectively. The shift in the 4th bending mode is negligible. The effect of different of mass ratios are presented in Table 5.

3.7. *Effect of input excitation level*

To study the behavior with respect to the excitation level of the input signal, the RMS value of the broadband random input signal is increased from 3.2 N to 56.2 N keeping the same bandwidth. The resulting transfer functions are given in Fig. 11.There is a decrease in the resonance peak in all the modes when input is less. As the input increases the transfer function approaches the transfer of function of the bare beam for higher modes except for the first mode where it has insignificant effect after 10 N RMS value. The likely reason could be that the same number of particles hit the walls of the cell in phase and out of phase resulting in negligible total momentum transfer from beam to particles.

Fig. 12 shows the snapshots of the particles in the cell at two different time instances at five locations. It can be seen that for the 56.2 N RMS input case, most of the particles remain in space most of the time without hitting the upper ceiling. As a result, interaction with structure is less and hence not only the effectiveness at very high input becomes negligible, the frequency shift also becomes negligible as the damping particles do not contribute to the modal effective mass.

3.8. *Effect of fill fraction with constant mass ratio*

To study the effect of fill fraction, all the parameters of the test including the PSD profile of the input, particle radius, total mass of the particles and other material properties are kept constant. Only the density of the particles is changed. Changing the density results in a change in the number of particles and volume and thus the fill fraction. Three cases are considered starting with acrylic particles with density 1180 kg/m^3 and particle radius of 1 mm. The transfer functions are shown in Fig. 13. As expected, there is no shift in resonance frequency with increasing density.

It can be concluded that the frequency shift is related to the added mass alone for a system of honeycomb cell where the space is very small and movement of the particles are highly constrained by the walls. There is insignificant effect on the magnitude of resonance peaks as the fill fraction or the numbers of particles are increased keeping the mass constant.

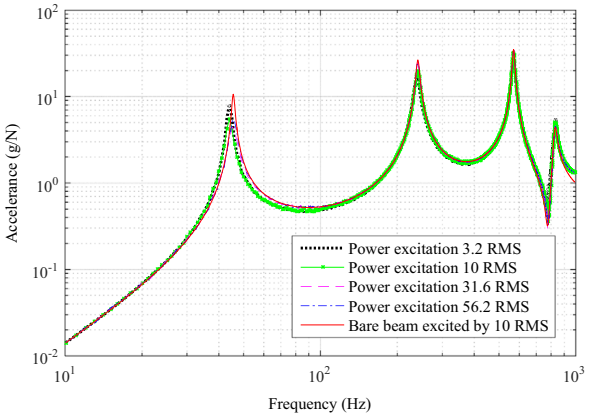

Fig. 11. Effect of excitation level.

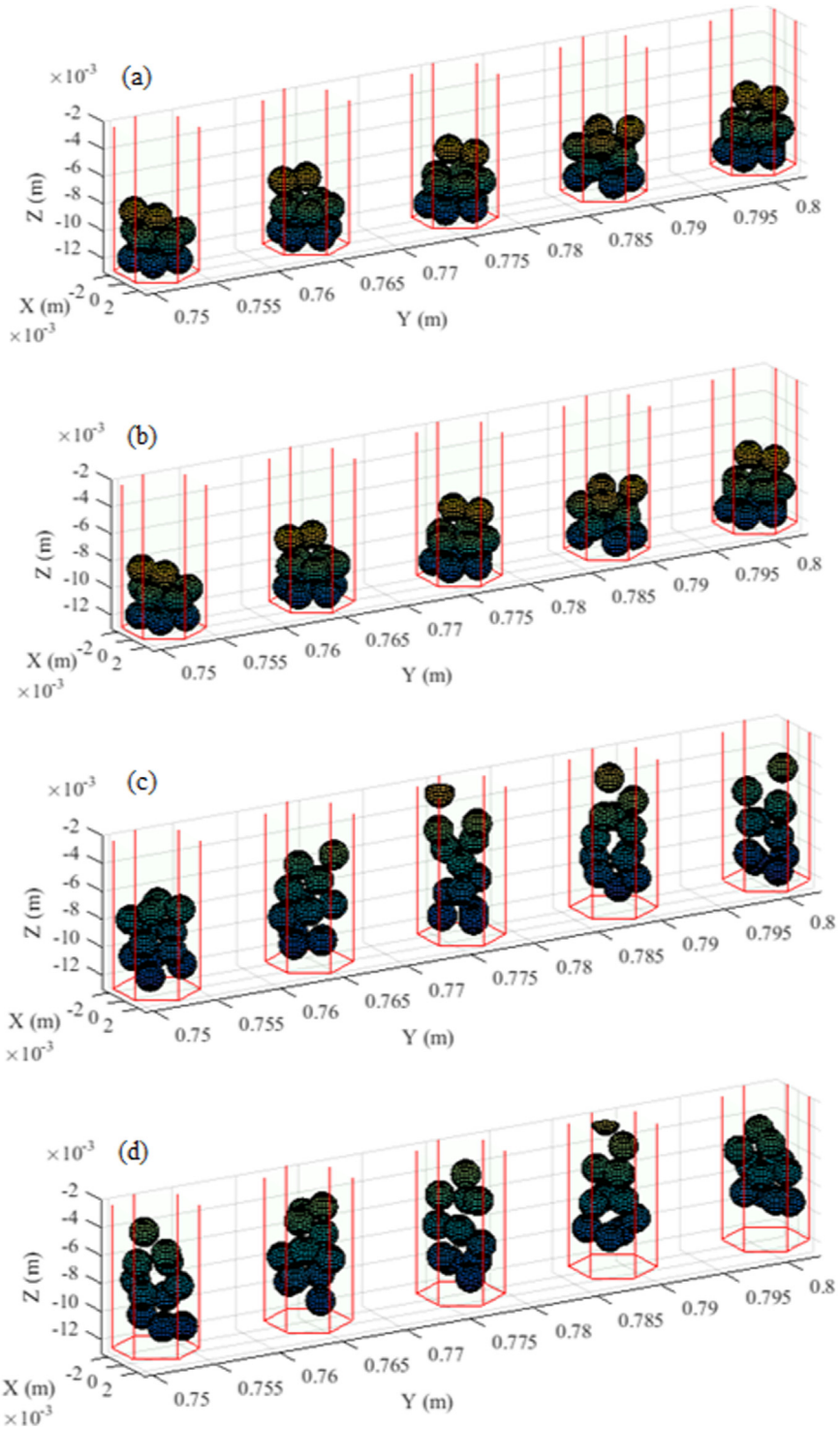

Fig. 12. Snapshots of the particles positions: (a) at 2.1 s with 3.2 N RMS input, (b) at 7.1 s with 3.2 N RMS input, (c) at 2.1 s with 56.2 N RMS input and (d) at 7.1 s with 56.2 N RMS input.

4. Conclusions

The effect of the damping particles on the transfer function, damping behavior and resonance peaks of the honeycomb sandwich beam whose cells near the tip were filled with damping particles was investigated analytically and experimentally. A cell level model of the honeycomb core and its interaction with damping particles, modeled by DEM, was developed.

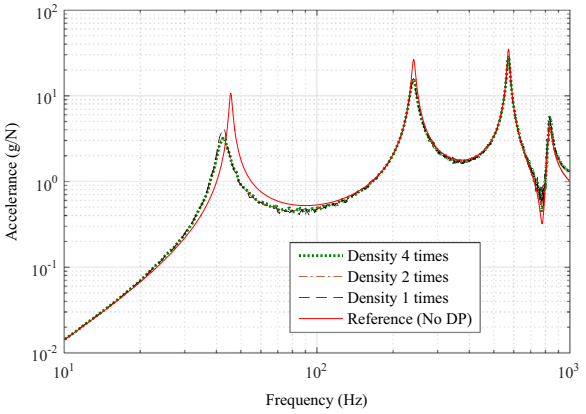

Fig. 13. Effect of fill fraction with constant mass ratio.

The model was validated by experimental work carried out on a cantilever beam that was subjected to random vibration input. The mathematical model was used to carry out parametric study with respect to fill fraction, mass ratio, excitation level and fill fraction with constant mass ratio. A monotonic decrease in the magnitude of resonance peaks was observed with increasing fill fraction for lower modes with different reduction for different modes. The reduction of frequency was also observed as the mass ratio was increased. It was observed that with lower value of excitation level there was decrease in the resonance peaks. However, for higher values, effect of damping particle on peak and shift in frequency was seen to be insignificant. With increasing fill fraction with constant mass ratio, there is no significant effect on the transfer function and no shift in frequency is observed.

Acknowledgement

The laboratory facilities and financial support from ISRO Satellite Centre, Bangalore, is highly appreciated. The authors would like to thank Mr. S Shankar Narayan, Head Experimental Structural Dynamics Division and Dr. K Renji, Group Director, Structures Group, at ISRO Satellite centre for their support and encouragements.

References

[1] B. Wang, M. Yang, Damping of honeycomb sandwich beams, *J. Mater. Process. Technol.* 105 (2000) 67–72.
[2] H.Panossian, Non-Obstructive Particle Damping: New Experiences and Capabilities, in: Proceedings of the 49th AIAA/ASME/ASCE/AHS/ASC Structures, Structural Dynamics, and Materials Conference, AIAA 2008–2102, Schaumburg, IL, 7–10 April, 2008.
[3] H.Panossian, Apparatus and method for aircraft cabin noise attenuation via non-obstructive particle damping, in: US 2005/0194210 A1, The Boeing Company, Chicago, IL, US, 2005.
[4] G. Michon, A. Almajid, G. Aridon, Soft hollow particle damping identification in honeycomb structures, *J. Sound Vib.* 332 (2013) 536–544.
[5] Z. Xu, M.Y. Wang, T. Chen, Particle damping for passive vibration suppression: numerical modelling and experimental investigation, *J. Sound Vib.* 279 (2005) 1097–1120.
[6] Z. Xu, M.Y. Wang, T. Chen, An experimental study of particle damping for beams and plates, *J. Vib. Acoust.* 126 (2004) 141.
[7] R. Vinayaravi, D. Kumaresan, K. Jayaraj, A.K. Asraff, R. Muthukumar, Experimental investigation and theoretical modelling of an impact damper, *J. Sound Vib.* 332 (2013) 1324–1334.
[8] S.F. Masri, T.K. Caughey, On the stability of the impact damper, *J. Appl. Mech.* 33 (1966) 586.
[9] S.F. Masri, General motion of impact dampers, *J. Acoust. Soc. Am.* 47 (1970) 229.
[10] M.R. Duncan, C.R. Wassgren, C.M. Krousgrill, The damping performance of a single particle impact damper, *J. Sound Vib.* 286 (2005) 123–144.
[11] Z. Lu, X. Lu, W. Lu, S.F. Masri, Experimental studies of the effects of buffered particle dampers attached to a multi-degree-of-freedom system under dynamic loads, *J. Sound Vib.* 331 (2012) 2007–2022.
[12] B. Yao, Q. Chen, Investigation on zero-gravity behavior of particle dampers, *J. Vib. Control* 21 (2013) 124–133.
[13] J.J. Moore, A.B. Palazzolo, R. Gadangi, T.A. Nale, S.A. Klusman, G.V. Brown, A.F. Kascak, A forced response analysis and application of impact dampers to rotordynamic vibration suppression in a cryogenic environment, *J. Vib. Acoust.* 117 (1995) 300.
[14] B.Knight, D.Parsons, A.Smith, R.Hunt, B.LaVerde, R.Towner, B.Craigmyle, Evaluating Attenuation of Vibration Response using Particle Impact Damping for a Range of Equipment Assemblies, in: AIAA Aerospace Design and Structures Event;8-11 Apr. 2013, Boston, MA, United States, 2013.
[15] N.Ahmad, R.Ranganath, A.Ghosal, Assessment of particle damping device for large laminated structures under acoustic excitations, in: Proceedings of the 14th ISAMPE National Conference on Composites (INCCOM-14), Hyderabad, 2016.
[16] C.J. Wu, W.H. Liao, M.Y. Wang, Modeling of granular particle damping using multiphase flow theory of gas-particle, *J. Vib. Acoust.* 126 (2004) 196.
[17] W. Liu, G.R. Tomlinson, J.A. Rongong, The dynamic characterisation of disk geometry particle dampers, *J. Sound Vib.* 280 (2005) 849–861.
[18] P.A. Cundall, O.D.L. Strack, A discrete numerical model for granular assemblies, *Géotechnique* 29 (1979) 47–65.
[19] M. Saeki, Analytical study of multi-particle damping, *J. Sound Vib.* 281 (2005) 1133–1144.
[20] M. Saeki, Impact damping with granular materials in a horizontally vibrating system, *J. Sound Vib.* 251 (2002) 153–161.
[21] C. Wong, M. Daniel, J. Rongong, Energy dissipation prediction of particle dampers, *J. Sound Vib.* 319 (2009) 91–118.
[22] K. Mao, M.Y. Wang, Z. Xu, T. Chen, Simulation and characterization of particle damping in transient vibrations, *J. Vib. Acoust.* 126 (2004) 202.
[23] X. Fang, J. Tang, H. Luo, Granular damping analysis using an improved discrete element approach, *J. Sound Vib.* 308 (2007) 112–131.

[24] Z. Lu, X. Lu, S.F. Masri, Studies of the performance of particle dampers under dynamic loads, *J. Sound Vib.* 329 (2010) 5415–5433.
[25] H.V. Panossian, Structural damping enhancement via non-obstructive particle damping technique, *J. Vib. Acoust.* 114 (1992) 101–105.
[26] H.Panossian, B.Kovac, R.Rackl, Composite Honeycomb Treatment via Non-Obstructive Particle Damping (NOPD), in: Proceedings of the 45th AIAA/ASME/ASCE/AHS/ASC Structures, Structural Dynamics & Materials Conference, AIAA 2004–1689, Palm Springs, California, 19 - 22 April, 2004.
[27] H.Panossian, R.Ehrgott, Non-Obstructive Particle Damping (NOPD) Treatment Optimization for Composite Honeycomb Panels, in: Proceedings of the 48th AIAA/ASME/ASCE/AHS/ASC Structures, Structural Dynamics, and Materials Conference, AIAA 2007–2047, Honolulu, Hawaii, 23 - 26 April, 2007.
[28] W. Goldsmith, *Impact*, Dover Publications Inc, Mineola, New York, 2001.
[29] Y. Tsuji, T. Tanaka, T. Ishida, Lagrangian numerical simulation of plug flow of cohesionless particles in a horizontal pipe, *Powder Technol.* 71 (1992) 239–250.
[30] R.D. Mindlin, H. Deresiewicz, Elastic spheres in contact under varying oblique forces, *ASME J. Appl. Mech.* 20 (1953) 327–344.
[31] N. Maw, J.R. Barber, J.N. Fawcett, The oblique impact of elastic spheres, *Wear* 38 (1976) 101–114.
[32] L. Vu-Quoc, X. Zhang, L. Lesburg, Normal and tangential force–displacement relations for frictional elasto-plastic contact of spheres, *Int. J. Solids Struct.* 38 (2001) 6455–6489.
[33] L. Vu-Quoc, X. Zhang, An accurate and efficient tangential force–displacement model for elastic frictional contact in particle-flow simulations, *Mech. Mater.* 31 (1999) 235–269.
[34] A.D. Lewis, R.J. Rogers, Experimental and numerical study of forces during oblique impact, *J. Sound Vib.* 125 (1988) 403–412.
[35] K.L. Johnson, *Contact Mechanics*, Cambridge University Press, Cambridge, 1985.
[36] S.E. Olson, An analytical particle damping model, *J. Sound Vib.* 264 (2003) 1155–1166.
[37] J. Wijker, *Mechanical Vibrations in Spacecraft Design*, Springer-Verlag Berlin Heidelberg GmbH, 2004.
[38] D.J. Ewins, *Modal Testing: Theory, Practice and Application*, Reaearch Studies Press Ltd., Hertfordshire, 2000.
[39] M. Baruch, Optimization procedure to correct stiffness and flexibility matrices using vibration tests, *AIAA J.* 16 (1978) 1208–1210.
[40] A. Berman, E.J. Nagy, Improvement of a large analytical model using test data, *AIAA J.* 21 (1983) 1168–1173.